15. R. H. Liu *et al.*, *J. Microelectromech. Syst.* **9**, 190–197 (2000).
16. H. Aref, *Phys. Fluids* **14**, 1315–1325 (2002).
17. Y. Z. Liu, B. J. Kim, H. J. Sung, *Int. J. Heat Fluid Flow* **25**, 986–995 (2004).
18. K.-I. Min *et al.*, *Angew. Chem. Int. Ed.* **49**, 7063–7067 (2010).
19. K.-I. Min, J. Im, H.-J. Lee, D.-P. Kim, *Lab Chip* **14**, 3987–3992 (2014).
20. K.-I. Min, J.-O. Kim, H. Kim, J. Im, D.-P. Kim, *Lab Chip* **16**, 977–983 (2016).
21. K. Fries, G. Finck, *Ber. Dtsch. Chem. Ges.* **41**, 4271–4284 (1908).
22. R. Martin, *Org. Prep. Proced. Int.* **24**, 369–435 (1992).
23. G. Bringmann *et al.*, *J. Org. Chem.* **67**, 5595–5610 (2002).
24. J. E. Semple, J.-F. Rossignol, Preparation of benzamide compounds as glutamate receptor modulators and therapeutic agents, PCT Int. Appl. WO 2012058378 (2012).

ACKNOWLEDGMENTS

Supported by National Research Foundation of Korea grants 2008-0061983, NRF-2015R1D1A3A01019112, and NRF-2014M1A8A1074940 and by Japan Society for the Promotion of Science Grant-in-Aid for Scientific Research (S) 26220804. Author contributions: H.K. and K.-I.M. conceived the concept at POSTECH; K.-I.M. fabricated the device; H.K. conducted synthetic experiments at POSETCH and Kyoto University with K.I.; D.J.I. conducted CFD simulation and analysis with K.-I.M.; and D.-P.K. and J.Y. directed the project.

SUPPLEMENTARY MATERIALS

www.sciencemag.org/content/352/6286/691/suppl/DC1
Materials and Methods
Figs. S1 to S3
Tables S1 to S6
NMR Spectra
References (*25*–*32*)

22 December 2015; accepted 28 March 2016
10.1126/science.aaf1389

GEOMORPHOLOGY

Self-organization of river channels as a critical filter on climate signals

Colin B. Phillips[1]* and Douglas J. Jerolmack[2]

Spatial and temporal variations in rainfall are hypothesized to influence landscape evolution through erosion and sediment transport by rivers. However, determining the relation between rainfall and river dynamics requires a greater understanding of the feedbacks between flooding and a river's capacity to transport sediment. We analyzed channel geometry and stream-flow records from 186 coarse-grained rivers across the United States. We found that channels adjust their shape so that floods slightly exceed the critical shear velocity needed to transport bed sediment, independently of climatic, tectonic, and bedrock controls. The distribution of fluid shear velocity associated with floods is universal, indicating that self-organization of near-critical channels filters the climate signal evident in discharge. This effect blunts the impact of extreme rainfall events on landscape evolution.

Understanding the control of climate on the geometry and erosion rate of rivers is essential for reconstructing the geologic history of landscapes and for predicting the response of rivers to human-accelerated climate change. A natural assumption is to link river erosion to climate through precipitation (*1*–*3*), yet demonstrating a clear relation is unexpectedly challenging (*4*–*7*). One reason is that bedrock river incision occurs primarily by abrasion due to the collision of particles with the stream bed (*8*) and "plucking" of loose blocks (*2*), and therefore it depends on sediment supply as well as precipitation. Another reason is that bedrock channel geometry both influences and adjusts to incision rate (*4*, *9*–*11*). The effects of climatic variability (*11*–*13*) and bedrock channel geometry (*9*, *10*) on river incision rates have been explored primarily with numerical models, but empirical observations remain limited.

In contrast to the case of bedrock systems, our understanding of the geometry of alluvial rivers (channels whose bed and banks are composed of mobile sediment) is built upon two empirically vetted theoretical principles. The first is "geomorphic work," in which the wide range of flows generated by climate—defined here as the magnitude, frequency, and phase of precipitation—is represented by a characteristic flood (*14*). This "bankfull" flood is the event whose frequency and magnitude combine to move the most sediment in the long-time limit, and it dictates channel size (Fig. 1). The second principle applies to gravel-bed rivers (median bed particle diameter, $D \geq 10$ mm), where sediment moves predominantly as bed load. Gravel-bed rivers adjust their geometry so that the width-averaged fluid shear velocity (U_*, meters per second) slightly exceeds the critical value (U_{*c}) at bankfull conditions. This is called the near-threshold channel, for which data and theory indicate that $U_*/U_{*c} \approx 1.1$ (Fig. 1) (*15*, *16*). Some studies, however, suggest that this treatment ignores details of climatic variability that may exert a substantial influence on landscape evolution (*1*, *17*, *18*). Observations reveal that the statistical distributions of discharge in many rivers possess a power-law tail (*12*, *13*, *19*), whose exponent changes with climatic setting (*17*). These observations have been interpreted to mean that channel shape may be controlled by climate and, for rivers with sufficiently heavy-tailed (log-log slope < −2) discharge distributions, that the rate of sediment transport could be dominated by extreme events due to climatic variability (*17*), which prevents rivers from achieving an equilibrium geometry over geologic timescales (*1*, *3*). Understanding the role of rivers in landscape evolution requires reconciling the proposed importance of climatic variability on channel form and dynamics with the apparent equilibrium behavior implied by near-universal hydraulic geometry scaling relations (*15*, *20*, *21*).

Climatic effects on river dynamics are typically characterized by discharge (Q, cubic meters per second), which is strongly related to precipitation (*22*), and erosion is often modeled using stream power (the product of discharge and slope, S). Bed-load motion, however, is driven by applied

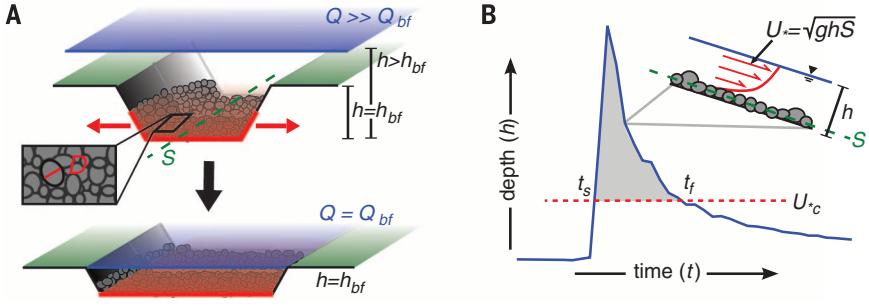

Fig. 1. Definition sketches. (**A**) Channel cross section illustrating adjustment to near-threshold bed-load transport; red regions are above the threshold of motion. The top panel shows flow exceeding bankfull conditions that induces transport on the banks, resulting in erosion and widening of the channel, which returns the system to near-threshold conditions (bottom). U_{*bf} was computed from channel surveys of S and h_{bf}. (**B**) Definition sketch of a flood, with relevant parameters shown. The gray shaded area (from the starting time t_s to the finishing time t_f) represents the part of a flood that is included in the integral for potential transport, which is calculated as $T = \int_{t_s}^{t_f} (U_*^2 - U_{*c}^2)^{3/2} dt/(gD_{50}^2)$ for $U_* \geq U_{*c}$ (*26*).

[1]St. Anthony Falls Laboratory, University of Minnesota, Minneapolis, MN 55414, USA. [2]Department of Earth and Environmental Science, University of Pennsylvania, Philadelphia, PA 19104, USA.
***Corresponding author. Email: colinbphillips@gmail.com**

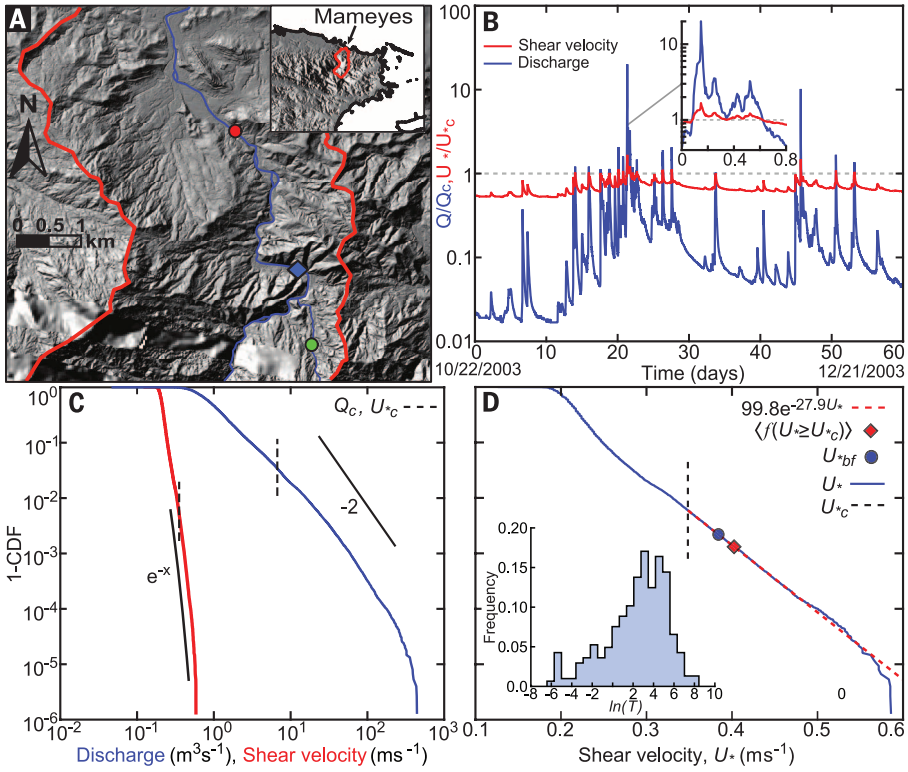

Fig. 2. The Mameyes River case study. (**A**) Lidar map of the Mameyes River catchment (red outline). The blue diamond shows the location of the USGS stream gage, and the red and green circles indicate the locations of the alluvial and the steep bedrock-alluvial tributary tracer studies, respectively. Flow is from south to north along the blue trace of the river. (**B**) Representative hydrograph from 2003 of discharge (blue) and shear velocity (red), measured every 15 min and normalized by the threshold of motion. The inset shows a single storm event. (**C**) Magnitude-frequency distribution of discharge (blue line, shown next to a slope of −2 for comparison) and of shear velocity (red line, shown next to an exponential function for comparison), indicating heavy-tail and thin-tail behavior, respectively (CDF, cumulative distribution function). A log-log slope shallower than −2 indicates infinite variance, meaning that a characteristic discharge cannot be obtained. (**D**) Magnitude-frequency distribution (semi-log scale) of U_* (blue line), which is well described by an exponential function for flows in excess of U_{*c}. The red diamond and blue circle represent bankfull shear velocity (U_{*bf}) and the average flood $\langle f(U_* \geq U_{*c}) \rangle$, respectively. The inset shows a PDF of ln(T).

fluid momentum represented by the shear velocity, $U_* = \sqrt{ghS}$, where g is gravity and h (in meters) is the width-averaged flow depth (Fig. 1B). For within-channel flows, shear velocity scales only weakly with discharge ($U_* \sim h^{1/2} \sim Q^{1/6}$) (*15*), and the relation is even weaker when flows exceed bankfull conditions and increases in Q contribute primarily to overbank flooding (*20*). We propose a set of parameters to examine the relations among hydrology, channel geometry, and bed-load transport for both bedrock and alluvial rivers, using a common framework: (i) the bankfull shear velocity, U_{*bf} (Fig. 1A); (ii) the distribution of floods, $f(U_* \geq U_{*c})$, characterized by the frequency-magnitude distribution of flows exceeding critical conditions (Fig. 2D); and (iii) the potential transport volume per unit width of bed load during a flood, T (Fig. 1B) (*23*). For bedrock-influenced rivers, the actual transport rate depends on the degree of alluvial cover and will be less than T, but T should nevertheless characterize the relative magnitude of different floods. We hypothesize that alluvial and bedrock-influenced gravel-bedded streams are near-threshold channels, and we predict that $U_{*bf}/U_{*c} \approx 1.1$ (*15*, *16*) and that peak sediment transport (T) occurs as a result of intermediate floods, not the largest floods (*14*).

We undertook a study of the Mameyes River in the Luquillo Critical Zone Observatory in northeastern Puerto Rico (Fig. 2A), which is subject to frequent large flash floods (*23*) due to orographic storms and hurricanes (*24*). We used tracer cobbles placed in a steep mixed bedrock-alluvial tributary ($S = 1.2 \times 10^{-1}$, $D = 120$ mm) and a lower-gradient alluvial reach ($S = 7.8 \times 10^{-3}$, $D = 110$ mm) to estimate U_{*c} for each site and to demonstrate that bed-load transport is proportional to T (*25*, *26*). Discharge records for the alluvial reach (Fig. 2A) show heavy-tailed (nonconvergent) scaling (Fig. 2C) (*27*). The data for the mixed bedrock-alluvial tributary are of insufficient duration for similar

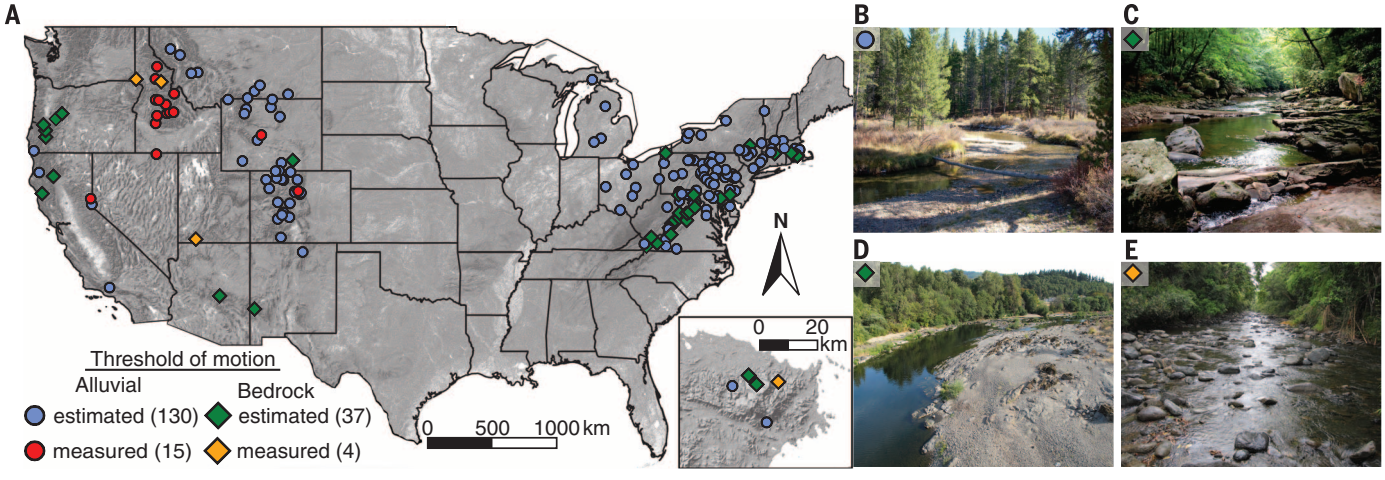

Fig. 3. Gaging stations used in this study. (**A**) Map of the continental United States and Puerto Rico (inset) with the locations of alluvial and bedrock-influenced stream gages used in this study (*26*), indicating where U_{*c} was measured or estimated. The easternmost gaging station in the map of Puerto Rico is the Mameyes River. (**B**) Halfmoon Creek ($S = 0.0084$, $D = 50$ mm), an alluvial-gravel river in the Colorado Rocky Mountains. (**C**) Bear Creek ($S = 0.021$, $D = 152$ mm), a bedrock-influenced river in Maryland. (**D**) Umpqua River ($S = 0.00067$, $D = 51$ mm), which drains a tectonically active region in the Oregon coastal and Cascade mountains. (**E**) Alluvial portion of the Mameyes River ($S = 0.013$, $D = 152$ mm). [Photo credits: D. N. Bradley (B), S. M. Baker and USGS (C), J. E. O'Connor (D)]

statistical analysis. Recorded peak discharges during flash floods can be up to 20 times the discharge associated with critical conditions (Q_c = 22 m^3 s^{-1}) (Fig. 2B). Although the threshold of motion is often exceeded more than 20 times per year (*28*, *29*), the associated shear velocity values for recorded floods are restricted to the range $U_{*c} \leq U_* \leq 2U_{*c}$ (Fig. 2B). Even the largest floods are near-threshold.

The frequency-magnitude scaling of U_* converges to an exponential function for above-critical values (Fig. 2D), and we computed $\langle f(U_* \geq U_{*c})\rangle / U_{*c}$ = 0.38 m s^{-1}/0.35 m s^{-1} = 1.1 (*23*), where the angle brackets denote the ensemble average value. The estimate for the channel-forming flood [$\langle f(U_* \geq U_{*c})\rangle$ = 0.38 m s^{-1}] is close to the bankfull shear velocity (U_{*bf} = 0.40 m s^{-1}) determined independently from morphologic surveys (*24*) of the channel (Fig. 1A); both are in agreement with near-threshold channel theory (*15*). As U_* approaches the maximum value, the tail decays faster than exponentially, indicating undersampling of the largest events (*27*, *28*). The probability density function (PDF) of T (Fig. 2D) possesses a peak, indicating the existence of a characteristic and moderate flood that transports the most sediment. Having shown that the hydrologic record of the mixed alluvial-bedrock Mameyes River displays near-critical behavior, we used measurements of channel geometry, slope, and grain size (fig. S1, A to E) (*23*) collected across bedrock and alluvial areas to test the generality of this result for the length of the river. Our calculations reveal that the ratio U_{*bf}/U_{*c} has no trend with downstream distance ($\langle U_{*bf}/U_{*c}\rangle$ = 1.3), despite substantial downstream decreases in channel slope and bedrock influence (fig. S1G), and indicates near-threshold transport throughout. Thus, an extreme distribution of discharge is not sufficient evidence to demonstrate control by infrequent, large flood events. The river's ability to adjust its width, depth, and grain size to near-critical conditions appears to decouple the distribution of U_* from the distribution of discharge imposed by climate. This critical filter confirms model predictions (*30*, *31*) that threshold sediment-transporting systems can shred external environmental signals.

We examined a wide range of gravel-bedded alluvial and bedrock-influenced streams located near U.S. Geological Survey (USGS) gages (*23*) across the United States (Fig. 3) to test the generality of the critical filter. The distributions of discharge [$f(Q \geq Q_c)$] vary widely among the rivers examined (Fig. 4A), as expected from previous research that indicates that this is predominantly an effect of spatial variation in climate (fig. S4) (*12*, *17*, *23*). In contrast, we can describe $f(U_* \geq U_{*c})$ with a global exponential function (Fig. 4B) (*23*). The average value for all streams is in agreement with near-threshold channel theory (*15*). Our data show that this characteristic flood magnitude is about equal to the morphologic U_{*bf} (Fig. 4C) (*23*), verifying the adjustment of both bedrock-influenced and alluvial rivers to the same near-critical conditions. The agreement is best for field sites where U_{*c} has been locally determined from observations (*23*), suggesting that much of the scatter in Fig. 4C is due to the notorious problem of estimation errors in determining the threshold of motion (*26*). We found a peak in T for all rivers that corresponds to moderate floods (Fig. 4C, inset), providing additional evidence that extreme events do not dominate channel form (fig. S7).

The rivers that we examined act as a filter, converting the wide range of climatically driven discharge distributions into a universal distribution of excess shear velocity. Flows greatly exceeding critical conditions cannot occur for long without leading to bank erosion, channel widening, and the restoration of flow conditions to near-critical (Fig. 1). This filtering is a logical consequence of the self-organization of rivers to a near-threshold channel geometry. We extend this reasoning beyond alluvial gravel-bedded rivers to bedrock-influenced rivers. The apparent generality of the critical filter calls into question the proposed links between extreme precipitation events, climate variability, and long-term river incision (*1*, *3*, *17*). Although large floods occur, they do not appear to control channel geometry for the rivers that we studied. An important caveat, however, is that we lack data for the steepest-slope rivers, where stream gages are rare, and for rapidly uplifting landscapes, where steep-walled gorges may violate our reported relations. The time scale of channel adjustment to external forcing is an important parameter, because this represents the time necessary to decouple $f(U_* \geq U_{*c})$ from discharge. Our results suggest that channel geometry has adjusted to the current hydrologic regime in almost all the rivers that we examined, even though some of these are influenced by bedrock. How, and for how long, this adjustment plays out is not well understood. Other studies have shown that alluvial (*29*) and bedrock (*32*) channels may respond to hydrologic perturbations on decadal time scales. Laboratory experiments (*33*, *34*) have demonstrated that coarse-grained bedrock channels may ultimately evolve their geometry and slope toward near-threshold transport conditions under an imposed sediment load. Although adjustments in the slope of natural rivers may take centuries to millions of years (*9*, *35*), our analysis indicates that channel geometry adjusts rapidly to accommodate bed-load transport under an imposed slope and grain size. Another possibility is that rivers with more resistant banks may sort sediment rapidly under an imposed channel geometry, so that the grain sizes remaining on the channel bottom are near-threshold for the bankfull flood. Both mechanisms of adjustment may be present within a single catchment (*32*). We suggest that landscape evolution models could

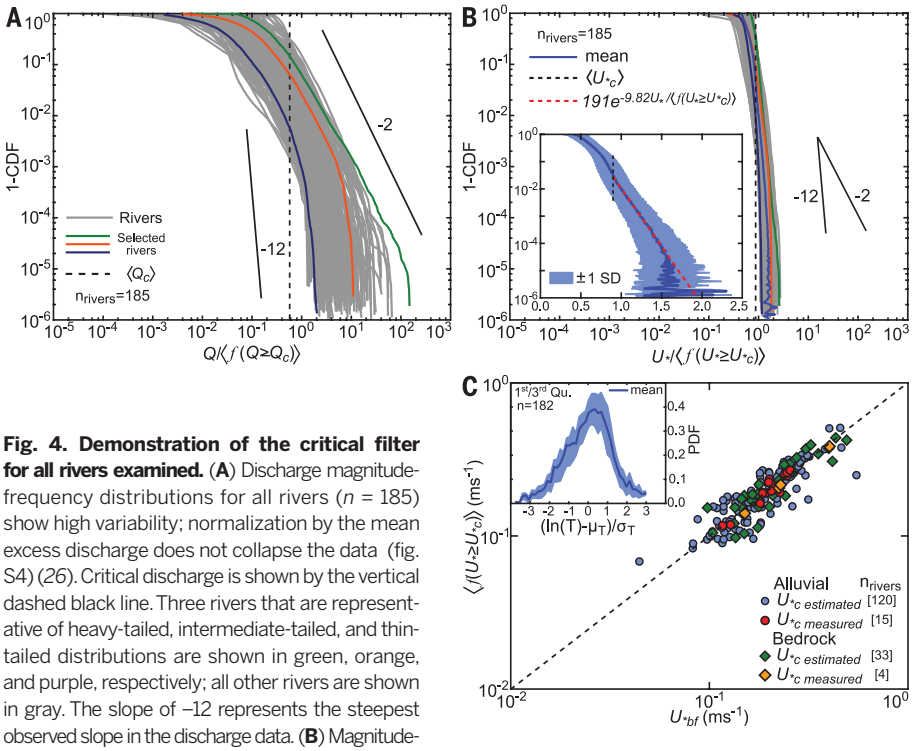

Fig. 4. Demonstration of the critical filter for all rivers examined. (**A**) Discharge magnitude-frequency distributions for all rivers (n = 185) show high variability; normalization by the mean excess discharge does not collapse the data (fig. S4) (*26*). Critical discharge is shown by the vertical dashed black line. Three rivers that are representative of heavy-tailed, intermediate-tailed, and thin-tailed distributions are shown in green, orange, and purple, respectively; all other rivers are shown in gray. The slope of –12 represents the steepest observed slope in the discharge data. (**B**) Magnitude-frequency distribution for $U_*/\langle f(U_* \geq U_{*c})\rangle$ for all stream gages, with same colors as (A); normalization by the mean reasonably collapses the data onto a single curve. The mean is indicated by the bold blue line. The inset shows the data on a semi-log plot, with light blue indicating ±1 SD. The dashed red line is an exponential fit to the mean for values of U_* greater than U_{*c} (dashed vertical black line). The tail decays faster than exponentially, indicating undersampling of the largest events (*27*, *28*). (**C**) Relation between $\langle f(U_* \geq U_{*c})\rangle$ and U_{*bf}, determined from independent surveys. The relation is strongest for rivers in which U_{*c} was measured. The inset shows the averaged distribution of T from all rivers, with light blue indicating the first and third quartiles (each river was standardized by using its mean μ and SD σ) (fig. S6). The peak indicates that moderate floods, and not extreme events, have sculpted the channels (fig. S7) (*26*).

implement a channel closure scheme by assuming $U_{*bf}/U_{*c} = 1.1$. In addition, a fixed-magnitude flood event with an intermittency factor (*36*) may be adequate for modeling the influence of climate on erosion over long time scales. Our results lend support to empirical studies that found that modest transport events perform the bulk of incision in bedrock-influenced rivers (*37*, *38*).

The critical filter that we have described here eliminates a substantial portion of the spectrum of environmental forcing, helping to explain how landscape patterns such as rivers remain stable in the face of highly stochastic driving. Channel adjustment decouples the sediment transport rate within a river from climatic influence. The delivery and removal of coarse sediment may determine the speed limit for river incision and landscape evolution (*8*), because bed-load transport remains near-threshold regardless of climate in bedrock-influenced and alluvial rivers.

REFERENCES AND NOTES

1. P. Molnar, *Annu. Rev. Earth Planet. Sci.* **32**, 67–89 (2004).
2. K. X. Whipple, *Annu. Rev. Earth Planet. Sci.* **32**, 151–185 (2004).
3. Z. Peizhen, P. Molnar, W. R. Downs, *Nature* **410**, 891–897 (2001).
4. D. W. Burbank *et al*., *Nature* **426**, 652–655 (2003).
5. K. X. Whipple, *Nat. Geosci.* **2**, 97–104 (2009).
6. K. L. Ferrier, K. L. Huppert, J. T. Perron, *Nature* **496**, 206–209 (2013).
7. B. J. Yanites, S. E. Kesler, *Nat. Geosci.* **8**, 462–465 (2015).
8. L. S. Sklar, W. E. Dietrich, *Geology* **29**, 1087–1090 (2001).
9. M. Attal, G. E. Tucker, A. C. Whittaker, P. A. Cowie, G. P. Roberts, *J. Geophys. Res.* **113**, F03013 (2008).
10. B. J. Yanites, G. E. Tucker, *J. Geophys. Res.* **115**, F04019 (2010).
11. G. E. Tucker, G. R. Hancock, *Earth Surf. Process. Landf.* **35**, 28–50 (2010).
12. D. Lague, N. Hovius, P. Davy, *J. Geophys. Res. Earth Surf.* **110**, (2005).
13. D. Lague, *Earth Surf. Process. Landf.* **39**, 38–61 (2014).
14. M. G. Wolman, J. P. Miller, *J. Geol.* **68**, 54–74 (1960).
15. G. Parker, P. R. Wilcock, C. Paola, W. E. Dietrich, J. Pitlick, *J. Geophys. Res.* **112**, F04005 (2007).
16. G. Parker, *J. Fluid Mech.* **89**, 127–146 (1978).
17. P. Molnar, R. S. Anderson, G. Kier, J. Rose, *J. Geophys. Res.* **111**, F02001 (2006).
18. R. A. DiBiase, K. X. Whipple, *J. Geophys. Res.* **116**, F04036 (2011).
19. D. L. Turcotte, L. Greene, *Stoch. Hydrol. Hydraul.* **7**, 33–40 (1993).
20. L. B. Leopold, M. G. Wolman, J. P. Miller, *Fluvial Processes in Geomorphology* (WH Freeman and Company, 1964).
21. D. R. Montgomery, K. B. Gran, *Water Resour. Res.* **37**, 1841–1846 (2001).
22. J. W. Kirchner, *Water Resour. Res.* **45**, W02429 (2009).
23. Materials and methods are available as supplementary materials on *Science* Online.
24. A. S. Pike, F. N. Scatena, E. E. Wohl, *Earth Surf. Process. Landf.* **35**, 1402–1417 (2010).
25. C. B. Phillips, R. L. Martin, D. J. Jerolmack, *Geophys. Res. Lett.* **40**, 1328–1333 (2013).
26. C. B. Phillips, D. J. Jerolmack, *Earth Surf. Dynam.* **2**, 513–530 (2014).
27. D. Sornette, *Critical Phenomena in Natural Sciences: Chaos, Fractals, Selforganization and Disorder: Concepts and Tools* (Springer, ed. 2, 2006).
28. D. J. Furbish, M. W. Schmeeckle, *Water Resour. Res.* **49**, 1537–1551 (2013).
29. L. J. Slater, M. B. Singer, *Geology* **41**, 595–598 (2013).
30. D. J. Jerolmack, C. Paola, *Geophys. Res. Lett.* **37**, L19401 (2010).
31. M. J. Van de Wiel, T. J. Coulthard, *Geology* **38**, 87–90 (2010).
32. J. P. L. Johnson, K. X. Whipple, L. S. Sklar, T. C. Hanks, *J. Geophys. Res.* **114**, F02014 (2009).
33. N. J. Finnegan, L. S. Sklar, T. K. Fuller, *J. Geophys. Res.* **112**, F03S11 (2007).
34. J. P. L. Johnson, K. X. Whipple, *J. Geophys. Res. Earth Surf.* **115**, (2010).
35. D. L. Egholm, M. F. Knudsen, M. Sandiford, *Nature* **498**, 475–478 (2013).
36. C. Paola, P. L. Heller, C. L. Angevine, *Basin Res.* **4**, 73–90 (1992).
37. K. Hartshorn, N. Hovius, W. B. Dade, R. L. Slingerland, *Science* **297**, 2036–2038 (2002).
38. J. R. Barbour *et al*., *Geophys. Res. Lett.* **36**, L04401 (2009).

ACKNOWLEDGMENTS

Research was supported by the NSF Luquillo Critical Zone Observatory (LCZO) (grant EAR-1331841 to D.J.J.), the NSF INSPIRE program (Integrated NSF Support Promoting Interdisciplinary Research and Education; grant EAR-1344280 to D.J.J.), and an NSF Postdoctoral Fellowship (grant EAR-1349776 to C.B.P.). We thank M. Brandon for encouraging this study; J. Willenbring, P. Wilcock, C. Paola, J. Kirchner, D. Furbish, and three anonymous reviewers for comments that improved this manuscript; and J. Buffington, W. Dietrich, G. Grant, J. O'Connor, A. Pike, J. Scheingross, M. Singer, L. Sklar, and J. Warrick for assistance in acquiring additional stream data. The authors declare that they have no competing financial interests. The data in this study are available from multiple sources: Field site data are compiled in table S1; all unprocessed stream gage data are freely available from the USGS National Water Information System; and lidar data are available from the LCZO. The Mameyes stream morphology and derived hydrograph data are available at https://figshare.com/authors/Colin_Phillips/644773.

SUPPLEMENTARY MATERIALS

www.sciencemag.org/content/352/6286/694/suppl/DC1
Materials and Methods
Figs. S1 to S7
Table S1
References (*39*–*91*)

29 August 2015; accepted 24 March 2016
10.1126/science.aad3348

POLYMER GROWTH

Uniform patchy and hollow rectangular platelet micelles from crystallizable polymer blends

Huibin Qiu,[1]*† Yang Gao,[1]* Charlotte E. Boott,[1]‡ Oliver E. C. Gould,[1]‡ Robert L. Harniman,[1]‡ Mervyn J. Miles,[2] Stephen E. D. Webb,[3] Mitchell A. Winnik,[4] Ian Manners[1]§

The preparation of colloidally stable, self-assembled materials with tailorable solid or hollow two-dimensional (2D) structures represents a major challenge. We describe the formation of uniform, monodisperse rectangular platelet micelles of controlled size by means of seeded-growth methods that involve the addition of blends of crystalline-coil block copolymers and the corresponding crystalline homopolymer to cylindrical micelle seeds. Sequential addition of different blends yields solid platelet block comicelles with concentric rectangular patches with distinct coronal chemistries. These complex nano-objects can be subject to spatially selective processing that allows their disassembly to form perforated platelets, such as well-defined hollow rectangular rings. The solid and hollow 2D micelles provide a tunable platform for further functionalization and potential for a variety of applications.

Nanoscale two-dimensional (2D) materials, typified by graphene and metal chalcogenide or clay nanosheets, are of broad utility. In principle, the solution self-assembly of block copolymers (BCPs) provides a convenient route to analogous planar nanostructures derived from soft matter (*1*, *2*). However, the formation of 2D platelet micelles is generally uncommon relative to other morphologies (*3*, *4*). Moreover, although considerable control has recently been achieved over the structures of 1D BCP micelles—in which fibers of tunable length and low dispersity (*5*, *6*) with periodic patches (*7*, *8*), block architectures (*9*), and amphiphilicity (*10*) are now accessible—progress with 2D assemblies is much more limited. Thus, the preparation of solid and hollow colloidally stable 2D micelles with similar fidelity and complexity remains a key challenge.

Self-assembly of BCPs with amorphous core-forming blocks in selective solvents provides a route to a diverse array of core-shell nanoparticles (micelles) with equilibrium or nonequilibrium morphologies of widespread utility (*3*, *4*). The most common morphologies formed are spheres, cylinders, and vesicles, and colloidal stability is provided by the presence of the solvent-swollen corona-forming block. The co-assembly or "blending" of different BCPs has recently been shown to provide a useful route to targeted conventional morphologies and also more complex nanostructures, such as disk-sphere or disk-cylinder hybrid micelles (*11*, *12*). As a result of their preference for the formation of rigid assemblies characterized by a core-corona interface with low mean curvature, BCPs with crystallizable core-forming blocks offer a promising route to planar

[1]School of Chemistry, University of Bristol, Bristol BS8 1TS, UK. [2]School of Physics, University of Bristol, Bristol BS8 1TL, UK. [3]Central Laser Facility, Science and Technology Facilities Council, Research Complex at Harwell, Rutherford Appleton Laboratory, Didcot OX11 0QX, UK. [4]Department of Chemistry, University of Toronto, Toronto, Ontario, M5S 3H6, Canada. *These authors contributed equally to this work. †Present address: School of Physical Science and Technology, ShanghaiTech University, Shanghai, 201210, China. ‡These authors contributed equally to this work. §Corresponding author. Email: ian.manners@bristol.ac.uk

Science
AAAS

Self-organization of river channels as a critical filter on climate signals

Colin B. Phillips and Douglas J. Jerolmack (May 5, 2016)
Science **352** (6286), 694-697. [doi: 10.1126/science.aad3348]

Editor's Summary

Filtering out the effect of large floods

Large floods should seemingly influence the depth and width of rivers. Phillips and Jerolmack, however, suggest that the self-organization of bedrock river channels blunts the impact of extreme rainfall events. River channel geometries from a wide range of course-grained rivers across the United States show that larger floods have very limited additional impact on channel geometry. River channel sculpting does increase as flood size increases, but the effect is most pronounced for moderate floods. This relationship may explain the long-term stability of rivers across shifts in climate.

Science, this issue p. 694

Science (print ISSN 0036-8075; online ISSN 1095-9203) is published weekly, except the last week in December, by the American Association for the Advancement of Science, 1200 New York Avenue NW, Washington, DC 20005.